Available online at www.sciencedirect.com
ScienceDirect
Icarus 190 (2007) 545–555
ICARUS
www.elsevier.com/locate/icarus

Lightning storms on Saturn observed by Cassini ISS and RPWS during 2004–2006

Ulyana A. Dyudina [a,*], Andrew P. Ingersoll [a], Shawn P. Ewald [a], Carolyn C. Porco [b], Georg Fischer [c], William Kurth [c], Michael Desch [d], Anthony Del Genio [e], John Barbara [e], Joseph Ferrier [e]

[a] *150-21, Geological and Planetary Sciences, Caltech, Pasadena, CA 91125, USA*
[b] *CICLOPS, Space Science Institute, 4750 Walnut Street Suite 205, Boulder, CO 80301, USA*
[c] *Department of Physics and Astronomy, University of Iowa, 203 Van Allen Hall, Iowa City, IA 52242, USA*
[d] *NASA-Goddard Space Flight Center, Code 695, Greenbelt, MD 20771, USA*
[e] *NASA/Goddard Institute for Space Studies, 2880 Broadway, New York, NY 10025, USA*

Received 13 November 2006; revised 14 March 2007

Available online 6 May 2007

Abstract

We report on Cassini Imaging Science Subsystem (ISS) data correlated with Radio and Plasma Wave Science (RPWS) observations, which indicate lightning on Saturn. A rare bright cloud erupt at ∼35° South planetocentric latitude when radio emissions (Saturn Electrostatic Discharges, or SEDs) occur. The cloud consisting of few consecutive eruptions typically lasts for several weeks, and then both the cloud and the SEDs disappear. They may reappear again after several months or may stay inactive for a year. Possibly, all the clouds are produced by the same atmospheric disturbance which drifts West at 0.45 °/day. As of March 2007, four such correlated visible and radio storms have been observed since Cassini Saturn Orbit Insertion (July 2004). In all four cases the SEDs are periodic with roughly Saturn's rotation rate (10^h39^m), and show correlated phase relative to the times when the clouds are seen on the spacecraft-facing side of the planet, as had been shown for the 2004 storms in [Porco, C.C., and 34 colleagues, 2005. Science 307, 1243–1247]. The 2000-km-scale storm clouds erupt to unusually high altitudes and then slowly fade at high altitudes and spread at low altitudes. The onset time of individual eruptions is less than a day during which time the SEDs reach their maximum rates. This suggests vigorous atmospheric updrafts accompanied by strong precipitation and lightning. Unlike lightning on Earth and Jupiter, where considerable lightning activity is known to exist, only one latitude on Saturn has produced lightning strong enough to be detected during the two and a half years of Cassini observations. This may partly be a detection issue.

Keywords: Lightning; Saturn, atmosphere; Atmospheres, dynamics; Meteorology; Spectroscopy

1. Introduction

The Cassini spacecraft attempted to detect lightning on Saturn by imaging and by radio signals. Although no direct light from lightning has been unambiguously detected so far, eruptions of a bright cloud can be seen in the images at latitude ∼35° South. Correlation of these eruptions with episodes of Saturn Electrostatic Discharges (SEDs) gives strong evidence of lightning on Saturn. This correlation had been noticed during the first half year of the Cassini mission in 2004 (Porco et al., 2005). The next two and a half years of Cassini observations confirmed that not only is the 35° South cloud present when SEDs are present, but also that this cloud is absent during order of year-long periods when the SEDs are absent. This paper reports all lightning-related imaging data collected by Cassini as of summer 2006, and analyzes the 35° South clouds in terms of reflectivity, vertical structure, and life cycle. All these details support the possibility of lightning in these clouds.

The two previous attempts to detect lightning on Saturn were made by the Voyager spacecraft. Voyagers 1 and 2 detected SEDs, which were also grouped into episodes, but the recurrence period was 10^h10^m (Kaiser et al., 1984) instead of 10^h39^m to 10^h41^m as in this study. The Voyager SEDs were in-

* Corresponding author. Fax: +1 (626) 585 1917.
E-mail address: ulyana@gps.caltech.edu (U.A. Dyudina).

0019-1035/$ – see front matter
doi:10.1016/j.icarus.2007.03.035

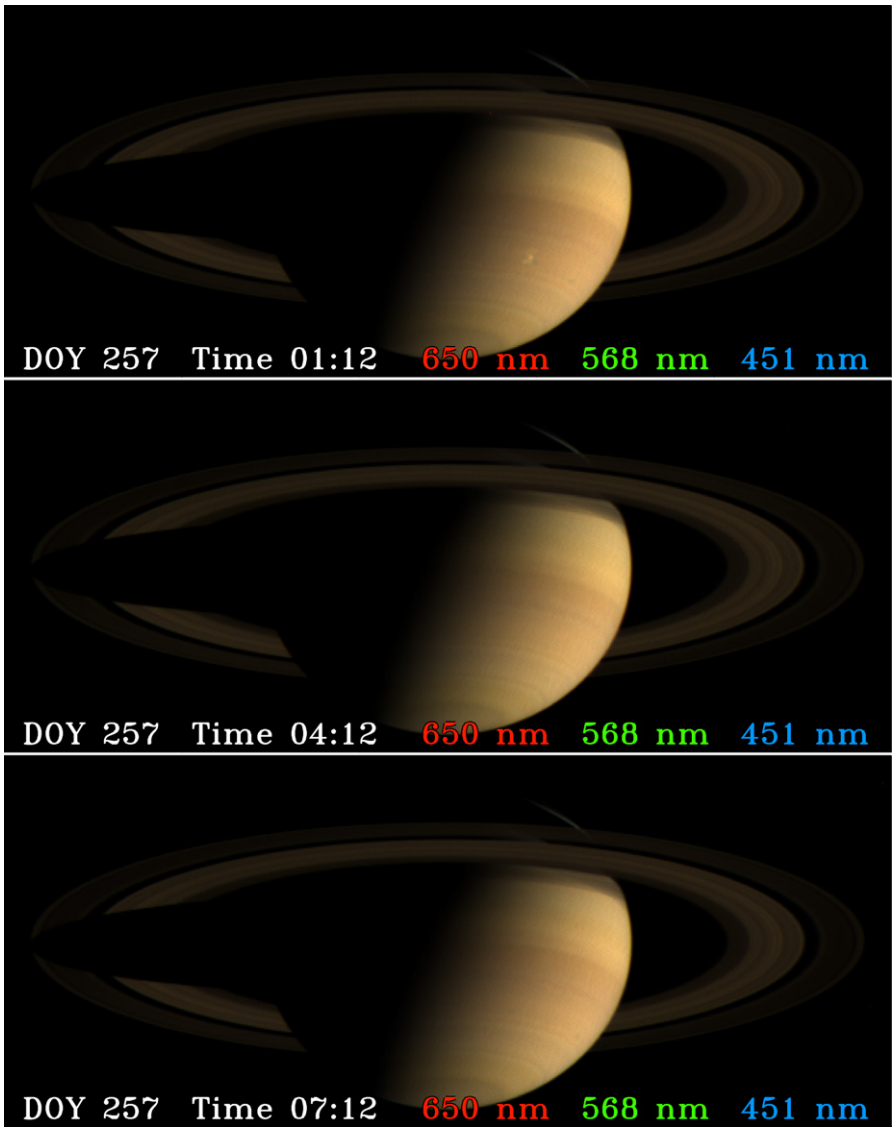

Fig. 1. A view of Saturn observed at three widely spaced longitudes during one saturnian day (true-color in the online version of the paper). Upper panel shows a unique extremely bright storm, which is active on the planet on that day. Images taken in combination of CL1 filter with the RED (central wavelength 650 nm), GRN (568 nm), and BL1 (451 nm) filters (Porco et al., 2004) are combined in the red, green, and blue color planes, respectively, of the output image. CL1 is a broadband clear filter used in the first of the two overlapping ISS filter wheels to minimize optical contribution from this wheel and study the wavelengths defined by the other filter in the second wheel. The day of year 2004 and time are shown in the lower left corner of each panel. The brightness for each filter is normalized by the incident solar light and is given in dimensionless reflectivity units of I/F displayed in the range of 0.02 to 0.61 in each color plane. The images are taken by the wide angle camera. A high-resolution narrow-angle camera view of the storm is shown in Fig. 2. (For interpretation of the references to color in this figure legend, the reader is referred to the web version of this article.)

terpreted as produced either in the rings or, more likely, in the atmosphere, i.e., by lightning (Burns et al., 1983; Kaiser et al., 1983). The correlation with clouds in Cassini ISS images gives convincing evidence that SEDs are produced by lightning.

Section 2 describes the clouds observed by ISS. Section 3 gives a brief introduction to the SEDs detected by Cassini. SED details can be found in a companion paper (Fischer et al., 2007). Section 4 shows that the several-week-long SED episodes are correlated with several-week-long episodes of clouds erupting at 35° South during the 2-year history of Cassini observations. Section 5 demonstrates the correlation of the times when SEDs are observed each saturnian day with the times when the clouds are seen.

2. Images of the storms taken by Cassini ISS

The Cassini ISS observed extraordinarily bright clouds appearing at latitude ∼35° South on Saturn four times between June 2004 and March 2007: three eruptions of the same storm in 2004 and another storm in 2006. Fig. 1 shows Saturn observed at three widely spaced longitudes during the same saturnian day when one such cloud erupted. The three observations cover most of Saturn's area. It is clear that the storm in the upper panel is unique on the planet. Most of the time Saturn does not have such storms and the atmosphere looks like the two lower panels. In the true-color version of this figure (see online version of this paper), the storm's color is similar to the brownish-orange

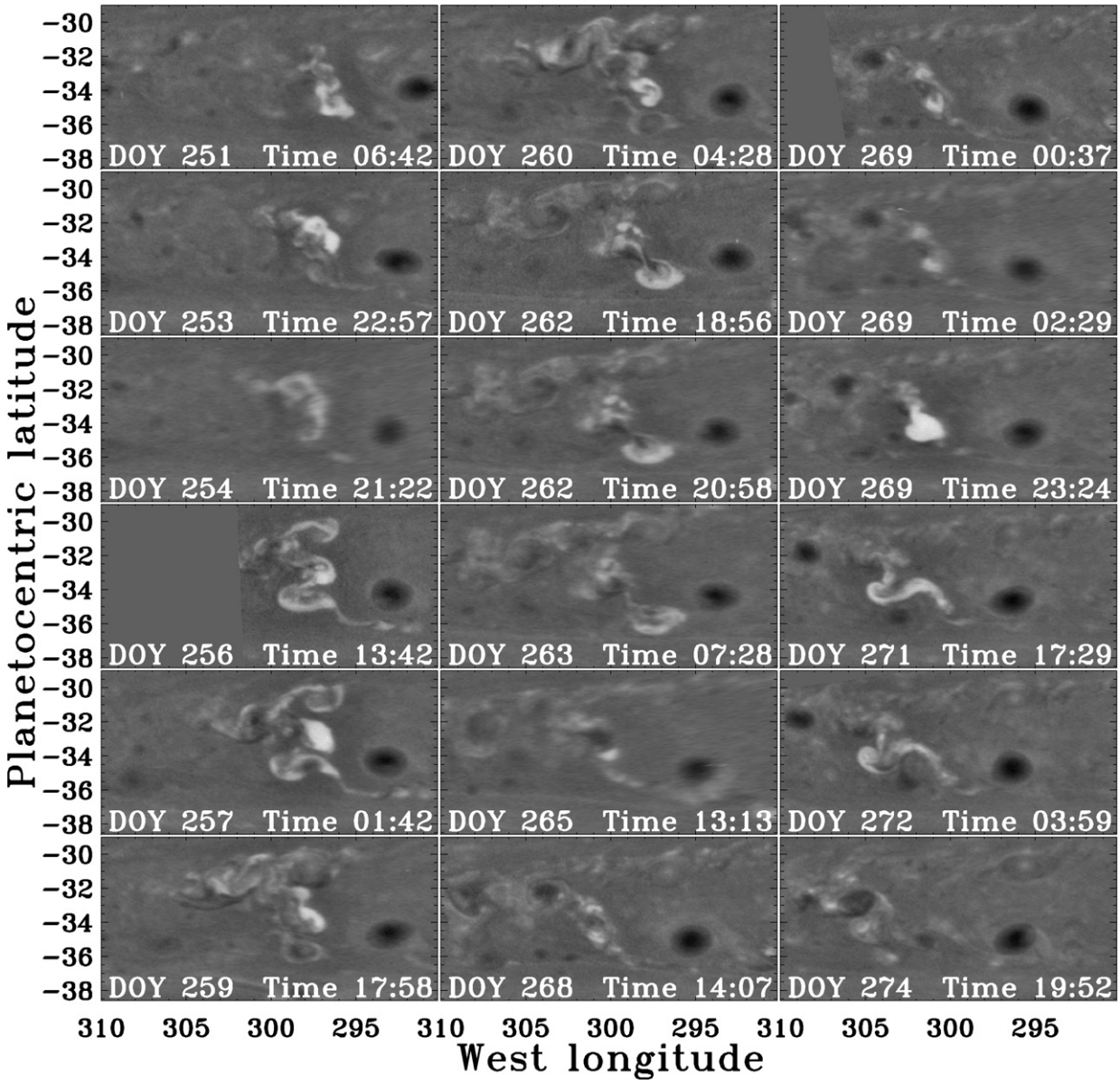

Fig. 2. Time sequence of the 2004 storm (time increasing from top to bottom plots and then to the next column). The maps are produced from the day side images taken in CL1, CB2 (750 nm) filter combination. The date of each map is shown in its lower left corner. One degree latitude is around 1000 km. The dimensionless residual brightness is shown as a shade of gray varying from −0.15 (black) to 0.25 (white) at the same scale for all images. Brightness variations derived from more images of this storm are plotted in Fig. 7.

color of the surrounding clouds. Extraordinarily bright storms appear on Saturn on the timescales of several years, e.g., similar storms at latitude 35° North were observed during Voyager 2 flyby (Smith et al., 1982; Sromovsky et al., 1983). Even larger probably convective storms sometimes referred as "Great White Spots" occur about every 30 years either at latitudes near equator, or 35° North, or 60° North (Sanchez-Lavega et al., 1991; Westphal et al., 1992). Smaller probably convective clouds are common on Saturn (Del Genio et al., 2006).

Porco et al. (2005) show the time sequence of the 2004 storm images in their Fig. 5. We improve this description in our Figs. 2 and 3. In Fig. 2 we normalize the image brightness such that the storm reflectivity can be viewed changing in time. We use color in Fig. 3 to show the cloud elevations as derived from images taken in different filters, which reveals the three-dimensional morphology typical for convective clouds.

Fig. 2 shows several Narrow Angle Camera (NAC) snapshots of the 2004 storm (see a description of Cassini cameras and filters in Porco et al., 2004). The 2004 storm started in July, lasted for at least a week, re-appeared in August, was not monitored by the ISS camera for ten days, and then was seen again in September. The July and August observations were taken by the Wide Angle Camera (WAC) at low resolution (∼500 km/pixel), which defined the position of the storm but not the fine structure. The September observations were taken by the Narrow Angle Camera (NAC) at high resolution (∼50 km/pixel). The brightness on the Fig. 2 maps is divided by the background brightness (i.e., by the same map low-pass

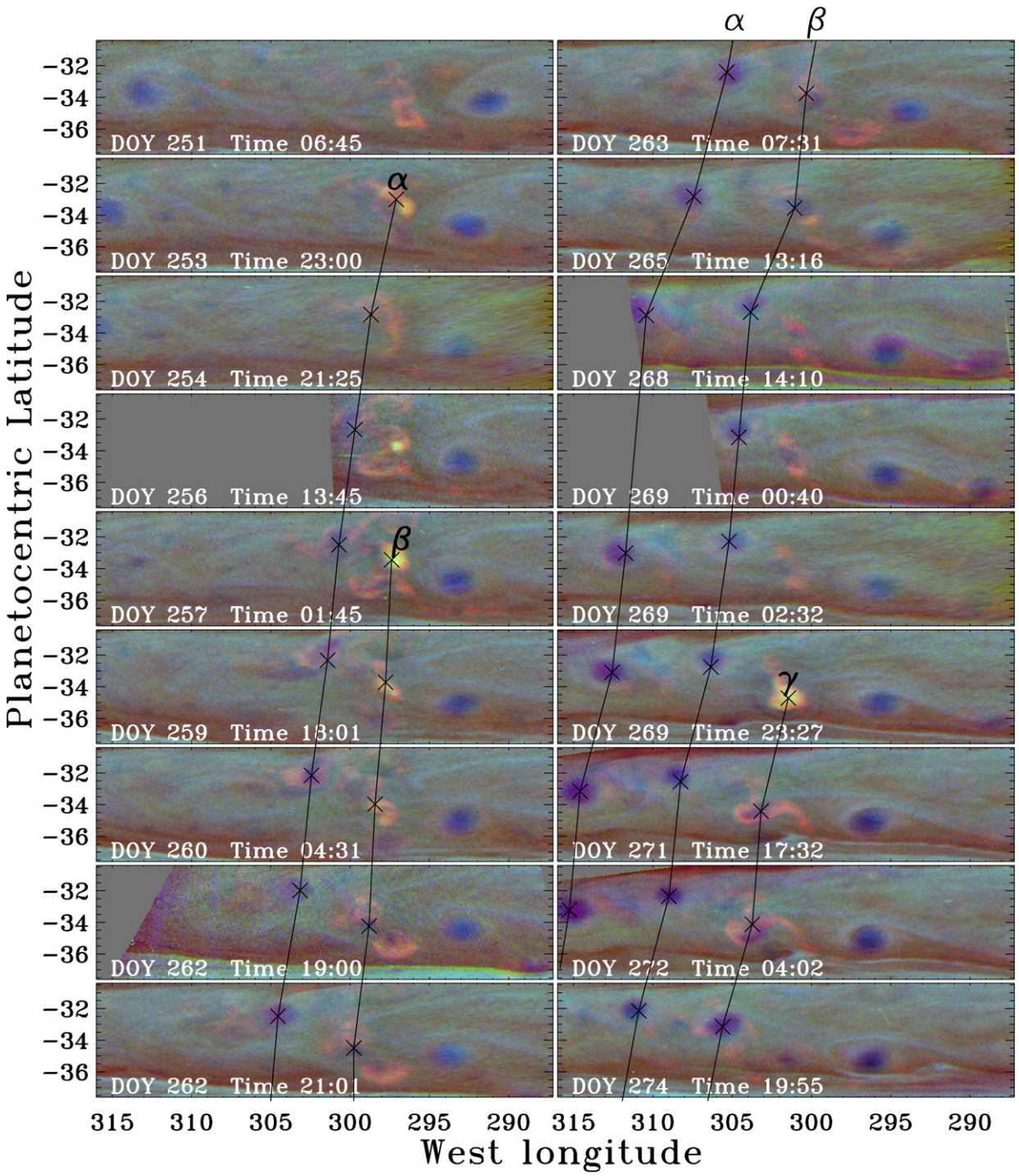

Fig. 3. False-color maps showing the cloud's depth variation with time. Color planes are combined from maps of the dimensionless residual brightness in filter combinations CL1 + CB2 (750 nm, red color plane), CL1 + MT2 multiplied by 3 (727 nm, green color plane), and CL1 + MT3 multiplied by 2 (889 nm, blue color plane). The range of residual brightness from dark to bright in each color plane is from −0.25 to 0.3 after the multiplication. The date of each map is shown in its lower left corner. The lines marked α, β, and γ indicate the life cycle of individual cloud eruptions evolving into blue ovals while drifting west. X-symbols indicate cloud locations on each map. (For interpretation of the references to color in this figure legend, the reader is referred to the web version of this article.)

filtered at a length scale of around 5°). Then unity is subtracted from this ratio to obtain the dimensionless residual brightness above the background.

During the 23 days shown in Fig. 2, the 2004 storm produced a 2000-km-scale plume of bright material three times (DOY 253, 256, and 269, solid white in Fig. 2). Each of the plumes then was slowly sheared apart by the winds and faded with time. The onset time of the plumes is less than a day. The DOY 257 plume grows from a small cloud to a 2 × 2 degree spot in 12 h between the DOY 256 and DOY 257 images. The DOY 269 plume appears in the area that was virtually cloud-free in the first of the two DOY 269 images 21 h before. The model of sat-

urnian convective clouds by Hueso and Sánchez-Lavega (2004) predicts few hour timescales for updrafts capable of bringing a large mass of volatile-rich air from the lower levels to the upper atmosphere. There the volatiles condense and produce opaque well-observable clouds. On Earth, fast moist updrafts are the most likely places to produce violent precipitation, electrical charges between precipitating particles, and lightning. The 2000-km scale of the saturnian cloud plumes is similar to the 1000-km scale of jovian plumes producing clusters of 100-km-scale individual lightning flashes (Little et al., 1999; Dyudina et al., 2004). These plumes are probably similar to the 25–2000-km-scale terrestrial Mesoscale Convective Systems (MCSs) (MacGorman and Rust, 1998). The multiple-storm MCSs provide most of the rainfall in the tropics and are major climate drivers on the Earth (Del Genio and Kovari, 2002).

Fig. 3 supports the updraft explanation of the plumes by demonstrating that the plumes reach high altitudes (see also Del Genio et al., 2006), and do so quickly. The color planes of the figure are composed from the images taken with filters sensitive to different altitudes in the atmosphere. The continuum narrow band filter CB2 (750 nm, red color plane) senses clouds and aerosols from the top of the atmosphere down to the deepest levels of the troposphere. The filter at weak methane absorption band MT2 (727 nm, green color plane) senses down to the intermediate depths. At this wavelength the absorption optical depth one occurs at 1.2 bars for a cloud-free atmosphere (Tomasko et al., 1984). The filter at the strong methane absorption band MT3 (889 nm, blue color plane) senses the highest part of the atmosphere. At this wavelength the absorption optical depth one occurs at 0.33 bars, just above the 0.4 bar upper boundary of the convective region (Tomasko et al., 1984). Although we can give qualitative estimate of the relative clouds height by combining CB2, MT2, and MT3 images here, exact cloud heights can only be derived from a thorough inverse radiative transfer model, which is out of scope of this paper. The map combined from these three color planes shows the deepest clouds as red, intermediate clouds as green, and the holes or absorbers in the lower clouds covered by high haze as blue. The high dense clouds would look white. The fresh 2004 storm plumes α, β, and γ (DOY 253, 257, and 269 in Fig. 3) do look white, and thus they are not only dense, but also are high-altitude clouds. A high-altitude cloud is the likely result of an updraft. Terrestrial thunderstorms usually form in updrafts overshooting the tropopause and produce unusually high thick clouds.

The plumes turn red with time. This indicates the disappearance of the high clouds revealing thick lower clouds. Later, each of the three plumes evolves into a blue-colored oval, which drifts west at the rate of 0.8°–0.9°/day (see the three lines tracking storms α, β, and γ in Fig. 3). The location where the fresh plumes erupt (which can be imagined as a line connecting the white-colored starting points of each of the three plumes) also drifts west, but at much slower rate of 0.2°/day (as will also be derived in Section 5). The production of dark (in CB2) ovals by convective clouds in the 2004 storm had been noticed by Porco et al. (2005) and Vasavada et al. (2006). Here we show how the vertical structure of the plume changes as it evolves into the dark oval. The blue color of the ovals indicates non-reflective main cloud deck covered with high haze. To be non-reflective, the main cloud deck may have a hole revealing some unknown absorbing atmospheric gases below. Alternatively, the main cloud deck may contain absorbing cloud particles. Convection explains why the plumes first rise high in the atmosphere. The buoyant convective updraft rises and overshoots some stable layers in the atmosphere. While rising, the volatile-loaded plume cools and the volatiles (ammonia and maybe water) precipitate. After the updraft runs out of energy, the upper clouds disappear first, followed by the lower thicker clouds (red) that can still be seen sheared apart by the winds several days later. Some volatiles probably brought to the uppermost levels of the atmosphere by overshooting remain there for a longer time forming a thicker haze above the dark oval.

Fig. 4 shows the nearly-simultaneous maps of the 2004 storm taken at eight different wavelengths. The spectral shape of the filters can be found in Porco et al. (2005). As discussed above, the narrow-band (5–20 nm wide) filters at methane absorption bands MT3, MT2, and MT1 probe different altitudes in the atmosphere. The map in MT3 does not show the 2004 storm unlike most of the maps taken in other filters. This means that the plume does not get substantially above the 0.4-bar upper boundary of the convective region. It can also be seen that the oval at ~307° W, −37° S, which looks dark in most maps, is bright in MT3 map. Thus, the high haze is thicker than the average above that oval. At weaker absorption bands (MT2 and MT1) the storm appears with more contrast. This indicates that the storm develops mainly in the lower and middle cloud levels (see also Del Genio et al., 2006). The fact that the storm is almost invisible in ultraviolet (UV3) and is faint in blue (BL1) is consistent with the conclusion from MT3 that the storm develops mainly in the lower and middle cloud levels. The map in 100-nm-wide UV3 filter at 343 nm is strongly influenced by the Rayleigh scattering in the atmosphere. The Rayleigh scattering optical depth τ_R, according to Tomasko et al. (1984), who assumes 94%/6% H_2–He mixing ratio and surface gravity of 950 cm/s^{-2}, can be approximated by their Eq. (6):

$$\tau_R \approx 0.0244\left(1 + 0.016\lambda^{-2}\right) P\lambda^{-4},$$

where the wavelength λ is given in μm and the pressure P is given in bars. According to that equation, the Rayleigh optical depth one is reached in 343 nm ultraviolet filter at 0.5 bars and in 451-nm blue filter at 1.6 bars. Ambient cloud optical depth above that 1.6 bar level should be relatively low because Pioneer polarimetry at similar blue wavelength (440 nm, Rayleigh optical depth one at 1.4 bars) shows a strong component of Rayleigh scattering by gas. In ultraviolet the scattered light should be even more dominated by Rayleigh scattering. Because the small bright plume can be seen in blue and not in ultraviolet, it is likely located between the corresponding 1.6 and 0.6 bar levels. The bright cloud filaments around the plume can be seen in blue filter, but not at such high contrast as in longer wavelengths. Because of that, these filaments are likely located at or right below the 1.6 bar level. Comparing continuum narrow band filters at different wavelengths (CB1 at 619 nm, CB2 at 750 nm, and CB3 at 938 nm) one can see that

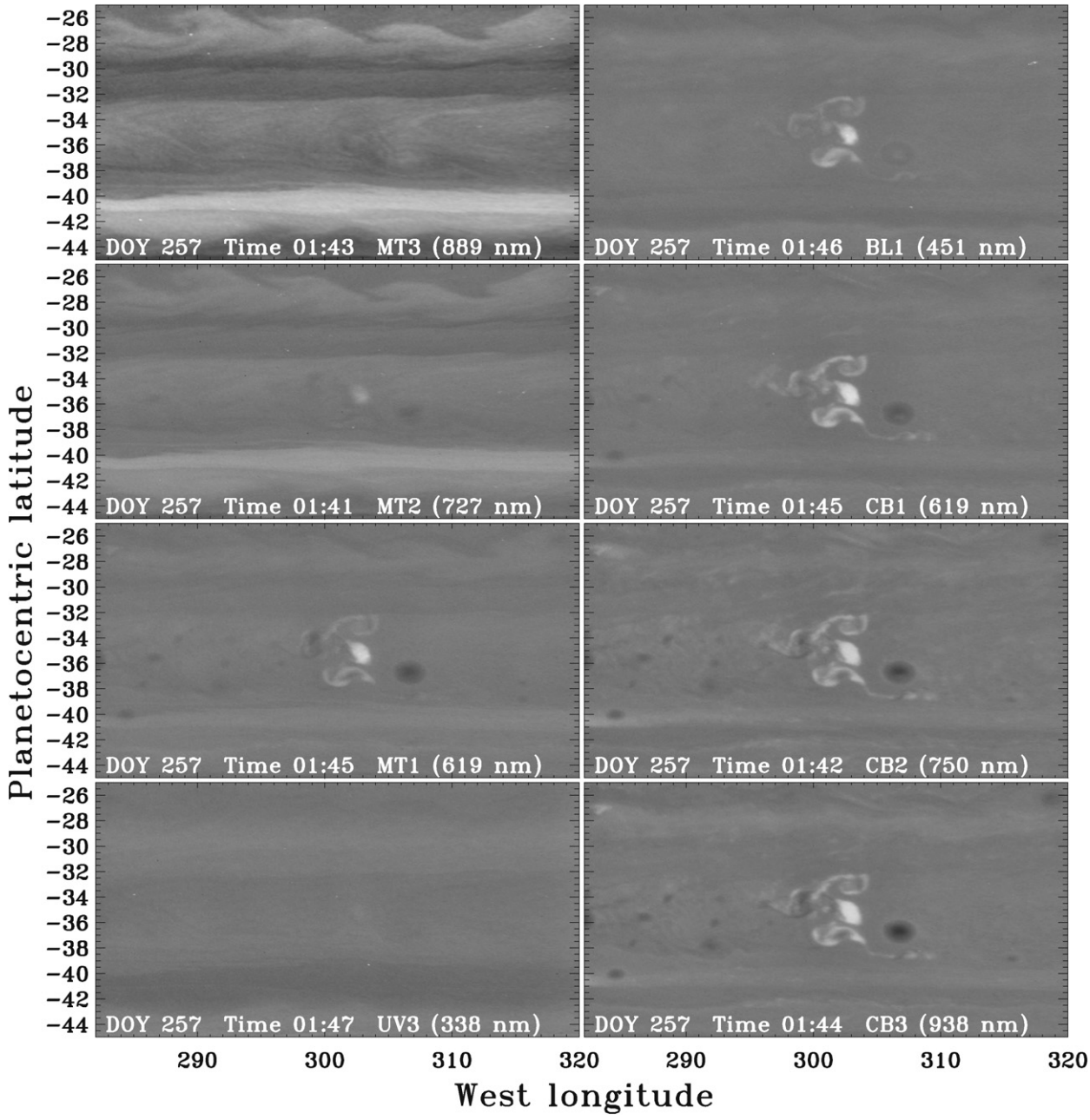

Fig. 4. View of the 2004 storm taken in different filters nearly simultaneously. The central wavelengths of the filters are: 619 nm for MT1, 727 nm for MT2, 889 nm for MT3, 338 nm for UV3, 451 nm for BL1, 619 nm for CB1 (which is a two-lobe filter with the gap at MT3 wavelengths), 750 nm for CB2, and 938 nm for CB3. Each of the filters is combined with a broadband filter on the other filter wheel, i.e. with CL1 or CL2 in the case of BL1. Maps of the dimensionless residual brightness are shown at the same scale for all filters as a shade of gray varying from −0.25 (black) to 0.35 (white). The date and time of each map and the filter names and wavelengths are shown at the bottom of each map.

the dark features have less contrast at shorter wavelengths. This may be due to the high haze of small particles having higher optical depth at shorter wavelength or Rayleigh scattering.

Fig. 5 shows the development of the 2006 storm. All the high-resolution images but the DOY 47 15:05 image are taken on the night side of the planet under the illumination of saturnian rings. The low-resolution images and the DOY 47 15:05 image are taken on the day side. All but the DOY 47 15:05 images in Fig. 5 are taken with a broad-band clear CL1 CL2 filter combination. The DOY 47 15:05 image is taken in narrow-band continuum CB2 filter, in which dark ovals similar to the ones in the 2004 storm are visible. The white plume shapes, sizes, and brightness are similar to the 2004 storm plumes. Three plume eruptions (solid white in Fig. 5) can be tracked in the history of this storm: the first one sometime between DOY 23 and 26 (because on DOY 26 there is a well-developed plume), the second on DOY 34–35, and the third on DOY 47. The three ovals are left over after the storm ends (see DOY 49). Their morphology and darkness in DOY 47 CB2 image confirms the similarity of the 2004 and 2006 storms.

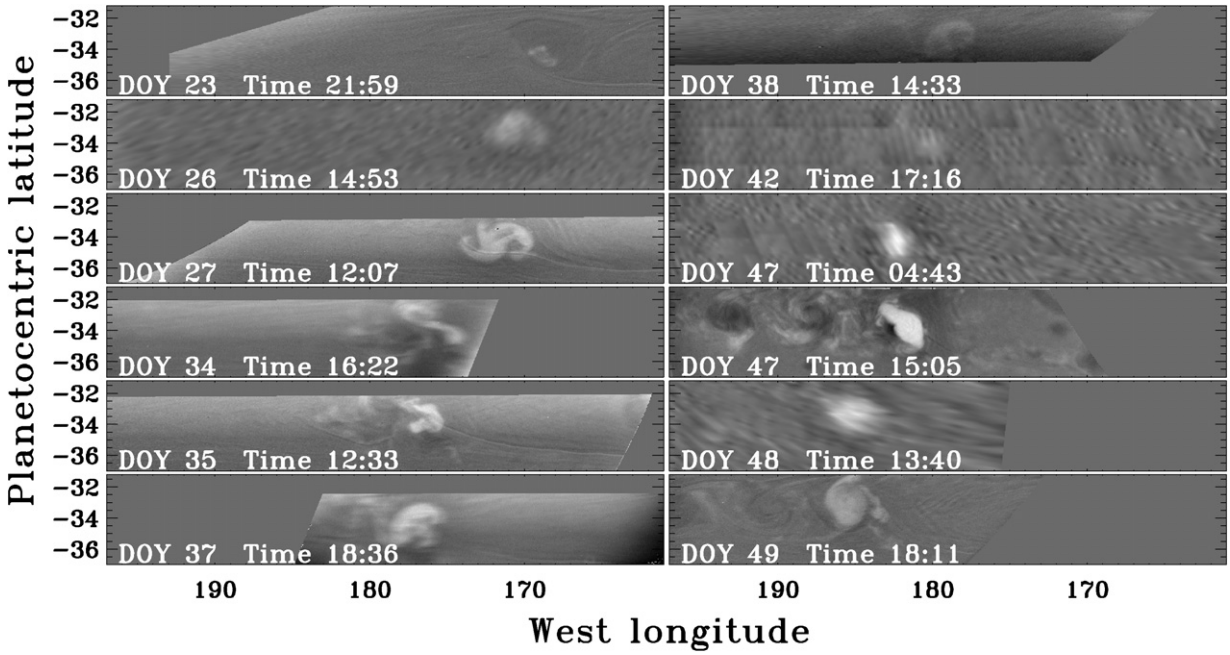

Fig. 5. Time sequence of the 2006 storm. The date of each map is shown in its lower left corner. High-resolution maps at DOY 23, 27, 34, 35, 37, 38, and 49 are produced from the night side images taken in CL1, CL2 filter combination. The image at DOY 47 time 15:05 is taken on the day side in CL1, CB2 filter combination. Low-resolution maps at DOY 26, 42, 47 (time 04:43), and 48 are taken on the day side in CL1, CL2 filter combination. The dimensionless residual brightness is shown as a shade of gray varying from −0.15 (black) to 0.21 (white) at the same scale for all maps. Brightness variation of the cloud with time can also be seen in Fig. 8.

3. Electrostatic discharges recorded by Cassini RPWS

The RPWS observations of the 2004 SEDs can be found in Fischer et al. (2006). Observations of the 2005 and 2006 SEDs can be found in the companion paper by Fischer et al. (2007). Here we briefly summarize those results and give the relation to the clouds reported in this paper.

During the storm eruptions, the Cassini RPWS instrument detected Saturn Electrostatic Discharges (SEDs). SEDs are short (tens of milliseconds in duration) electrostatic bursts spanning ∼1–16 MHz in frequency. The SEDs are grouped into episodes that recur with a periodicity close to Saturn's rotation. Most episodes last less than half of Saturn's rotation period (see Fig. 4 of Fischer et al., 2007). This periodic on-off pattern is consistent with SEDs originating at some small location in Saturn's atmosphere, which is observed by RPWS when this location is rotated into the Cassini-facing side of Saturn. The SED intensity variation during each saturnian rotation is consistent with partial damping of the signal from a small atmospheric source by the ionosphere. The SED low frequency cutoff during each saturnian day also favors the SED's atmospheric origin Zarka et al. (2006), Fischer et al. (2007).

In addition to the SEDs observed during the storms in 2004 and 2006, in 2005 RPWS observed one short SED storm containing a smaller number of SEDs. The SEDs during the 2005 episode had characteristics (frequencies, burst rates) similar to the ones in 2004 and 2006, but their periodicity is less clearly correlated with Saturn's rotation. Also, the duration of one of the 2005 SED episodes is 9 h, which substantially exceeds half of Saturn's rotation. This is inconsistent with a single small storm producing SEDs. Unlike the 2006 and 2004 SEDs, the 2005 episodes do not reappear every Saturn's rotation, but are rather sparse. The origin of the 2005 SEDs is puzzling because of such timing. Fischer et al. (2007) find a periodicity in the 2005 SEDs at $10^h 10^m \pm 10^m$. This period may be consistent with multiple equatorial thunderstorms.

Several moderately bright clouds are seen a few days after the 2005 SED maximum near the equator (between 0° and 10° South). These clouds are not clearly correlated with the SEDs on the timescale of days and hours (Fischer et al., 2007). This does not exclude the possibility that equatorial clouds produce the 2005 SEDs. The absence of correlation may be due to non-regular SED timing, large number and short lifetimes of the individual equatorial clouds, and sparse ISS coverage.

Three more cloud eruptions near latitude 35° South were observed by ISS before the Cassini Saturn orbit insertion on DOY 359 of 2003, on DOY 90 of 2004, and on DOY 111 of 2004, but RPWS did not detect SEDs, perhaps because of the large distance to Saturn (1500, 770, and 607 R_S, respectively).

A few more episodes of SEDs were observed in May 2004 from DOY 147–152. No extraordinarily bright clouds were observed on these days, which had a good coverage by ISS images with the exception of the ring-shadowed Northern hemisphere.

4. Three-year history of the storms and SED observations

Although quantifying the presence of very bright clouds among less bright clouds on Saturn is somewhat subjective, the extraordinarily bright clouds at 35° South are clearly distinct from the usual cloud coverage (see Fig. 1). Fig. 6 shows that the SEDs (black on the upper plot) and these bright clouds (black on the lower plot) are well correlated in time, i.e., when there

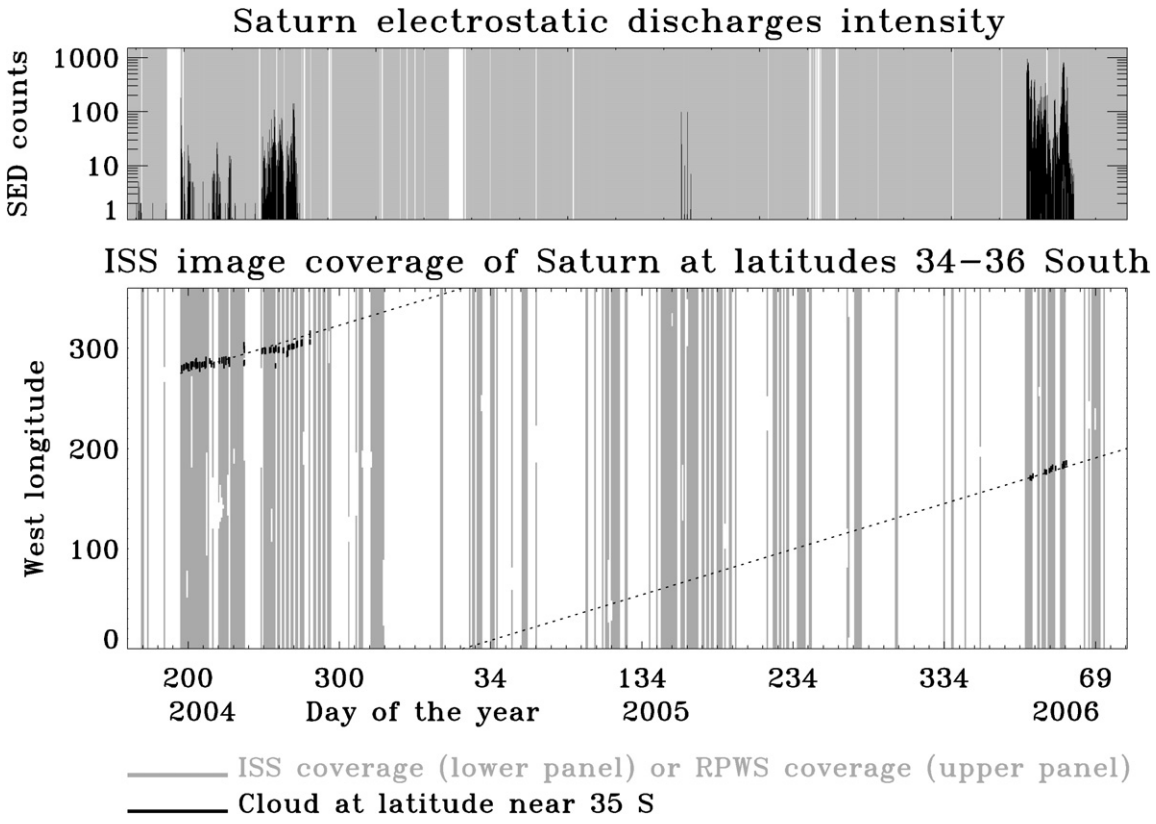

Fig. 6. Long-term correlation of SEDs and clouds on Saturn. Upper panel: SED counts in 2004–2006 plotted versus day of year in black (same abscissa as in the lower panel). RPWS was monitoring SEDs nearly continuously. Coverage of RPWS observations is shown in gray on the plot. Gaps in observations are shown in white. Lower panel: Times and longitudes when we believe that ISS is seeing thunderclouds are shown as black vertical lines on the plot. Each of the black lines extends 5 degrees in longitude. Grey indicates the coverage of ISS observations, i.e., times when Cassini ISS took images of Saturn's surface at the planetocentric latitudinal band 34°–36° South and was capable of detecting thunderclouds there. Gaps in ISS observations are shown in white. The slant dotted line connects 2004 and 2006 clouds as if they were eruptions of the same atmospheric disturbance drifting West at 0.45°/day.

are SEDs there is a cloud, and when there are no SEDs there is no cloud. Since January 2006 until March 2007 there were no SEDs and no cloud. The only exception from this correlation is the weak SED episode in 2005. As seen in the lower plot, this episode is not accompanied by a cloud at 35° South even though this latitude was well covered by the imaging. Moreover, no other location on the planet showed extraordinary bright clouds at that time, including the equatorial region proposed as a source of 2005 SEDs by Fischer et al. (2007). The moderately bright clouds observed a few days after the 2005 SEDs near the equator (see Section 3) are much fainter than the 2004 and 2006 storms. Also the number of detected SEDs is substantially smaller compared to the other big storms. It should be noted, though, that ISS did not see the entire planet. A substantial part of the Northern hemisphere was permanently covered by ring shadow, and we may have missed SED-producing clouds from that part of Saturn.

The lower plot of Fig. 6 shows the longitude of the observed clouds as the ordinate. The longitudinal extent of the cloud at each sighting was prescribed to be 5°, which is the longitudinal extent of the largest of the clouds. Both 2004 and 2006 clouds drift west (towards larger longitudes). The dotted line is an attempt to see if the atmospheric disturbance which created 2004 clouds continues drifting west until it erupts again in 2006. The line connects the 2004 and 2006 storm without taking into account the drift rates within each of 2004 or 2006 episodes. The 2004 cloud data span 80 days. During that time the drift rate of the black lines changes several times. With that uncertainty the drift rate may be consistent with the dotted line, but the fit is not perfect. The drift of the 2006 cloud is also consistent with the dotted line, but the uncertainty is large due to the short storm duration. As a result, we cannot unambiguously determine that the 2004 and 2006 storms are produced by the same atmospheric disturbance drifting west at 0.45°/day, although the data do not contradict such a possibility.

5. Correlation between clouds and SEDs relative to Saturn's rotation

Fig. 7 shows the correlation of the times when the 2004 storm crosses the sub-spacecraft (or central) meridian (CM) with the times of SEDs for each of its three active periods. On each image that contained the storm (a sighting), we measured the storm's longitude and computed when it would have crossed the CM on that saturnian day. The asterisk indicates the time of CM crossing (abscissa) and the excess reflectivity of the storm (ordinate) in the normalized units of excess reflectivity ((storm/surroundings) −1). Several asterisks at the same CM crossing represent several sightings of the storm on the same Saturn rotation. The different values of excess reflectivity on

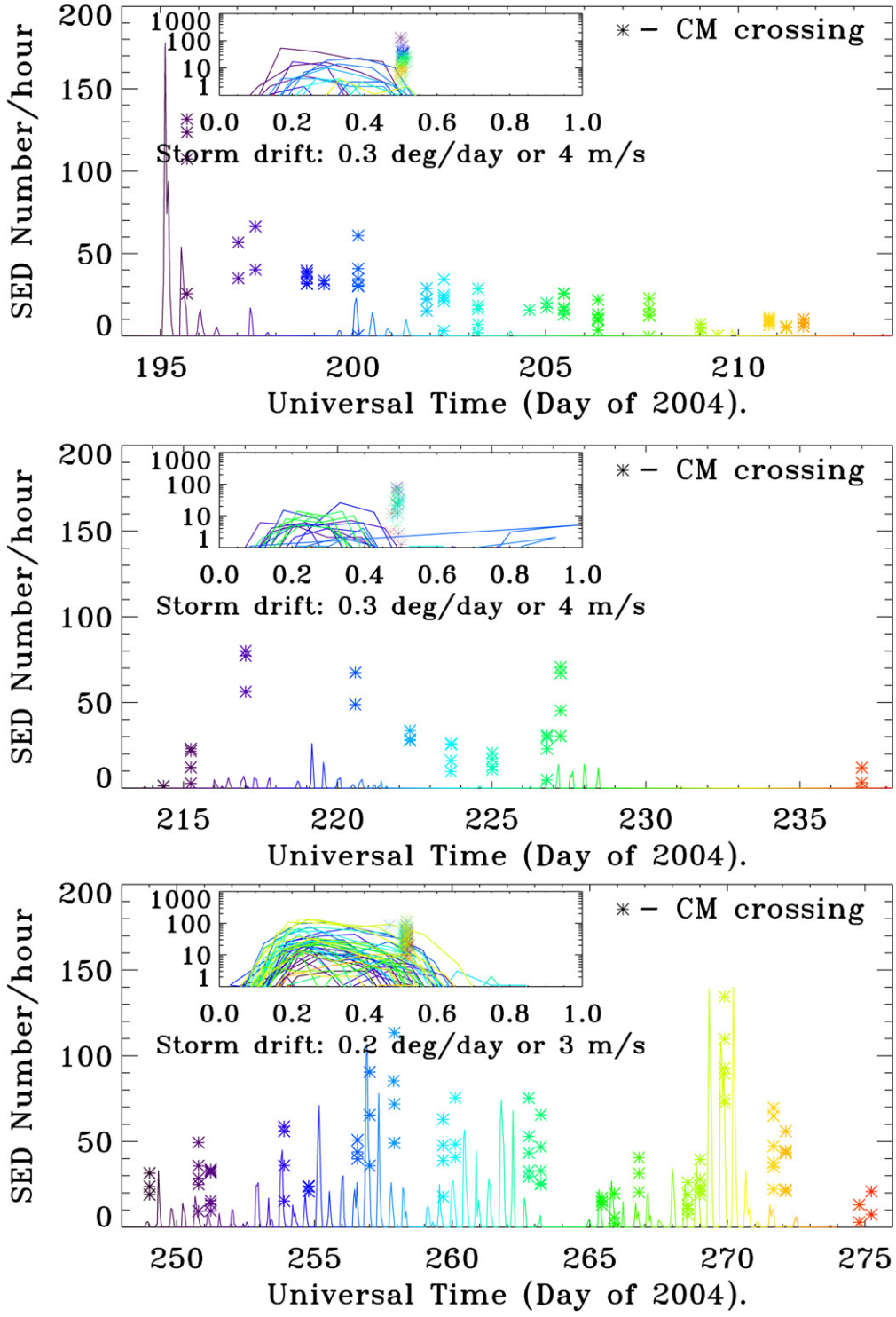

Fig. 7. Timing of the storms CM crossings relative to the timing of the SEDs for the year 2004. The abscissa is Universal Time at the spacecraft; the labels refer to the start of each day. For the solid curves, the ordinate both of the main plots and insets is the number of SED bursts per hour. The asterisk indicates the time of CM crossing (abscissa) and the excess reflectivity of the storm (ordinate showing the excess reflectivity times 500). The insets show the same data plotted versus the rotation period of the storm. The color indicates the date of the observation. The storm rotation periods for the drift rates of 0.3°/day and 0.2°/day are 10.661^h and 10.660^h, respectively.

the same Saturn rotation arise because the storm was observed at different positions on the variously-illuminated disk. Day 195 is July 13, day 215 is August 2, and day 250 is September 6, 2004. The upper, middle, and lower panels show SED storms A, B, and C from (Fischer et al., 2006), respectively. Fig. 8 shows the same SED/CM crossing correlation for the 2006 storm. The coverage of the storms was intermittent (see Fig. 6), so gaps in the asterisks represent Saturn days when there were no observa-

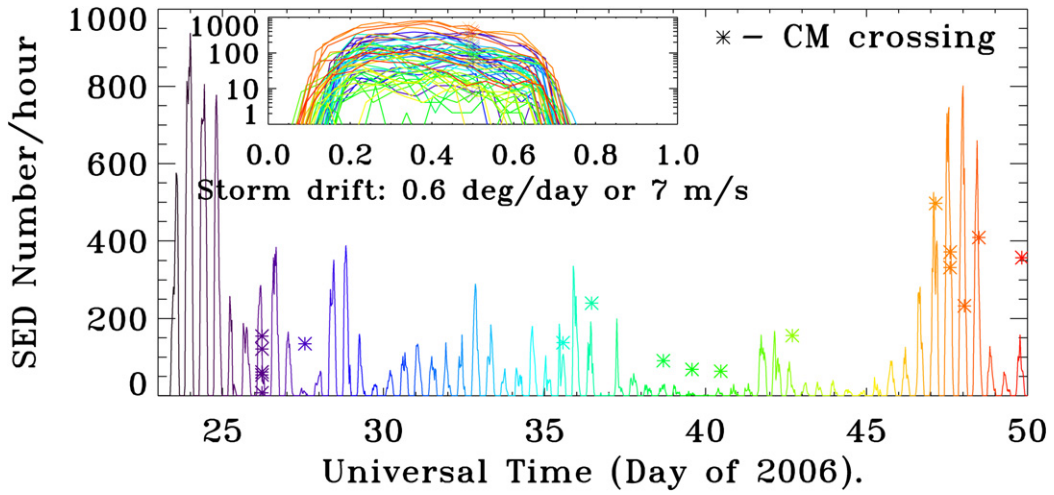

Fig. 8. Timing of the storms CM crossings relative to the timing of the SEDs for the year 2006 displayed the same way as in Fig. 7, but the ordinate for the asterisks shows the excess reflectivity times 2000. For the cloud brightness we use the Wide Angle Camera images showing the storm on the day side in filter combination CL1, CL2. The storm rotation periods for the drift rates of 0.6°/day is 10.665^h.

tions. The coverage of SEDs was nearly continuous (see Fig. 6), so gaps in the SED sequence represent Saturn days when there were no SEDs.

The maxima in the burst rates of the SED episodes at days 217–221, 227, 256, and 270 of 2004 (Fig. 7) and 25–35 and 46–48 of 2006 (Fig. 8) are correlated with brightening of the storm (see also the images of the clouds in Figs. 2, 3, and 5). This is additional evidence of a connection between SEDs and clouds.

Figs. 7 and 8 are similar to Fig. 6 from Porco et al. (2005), which displays part of our Fig. 7 data. We show more 2004 data in Fig. 7, middle panel, and new 2006 data in Fig. 8. All of the cloud data in this paper are reprocessed to show the excess reflectivity. All SED data are reprocessed to finer time grid of half an hour. Also we color-code the date at which both cloud and SED data were taken to track the date in the inset plots.

The insets show the same data as the main plots but plotted versus rotational phase using the period at which the storm rotates with Saturn's atmosphere. This period varies from storm to storm from 10.660–10.661^h in 2004 to 10.665^h in 2006. This is between Saturn Kilometric Radiation (SKR) rotation period measured by Voyagers ($10^h39^m24^s \pm 7^s$ or 10.6562^h) and the SKR rotation period measured by Cassini ($10^h45^m45^s \pm 36^s$ or 10.7625^h, Gurnett et al., 2005). We fitted the storm rotation periods for each of the 2004 and 2006 plot insets such that all the CM crossings (asterisks) from different days fit the same rotational phase of around 0.5. The corresponding westward drift rates of the storm relative to Voyager rotation period are shown below the inset plots. The uncertainty of the drift is around 0.1°/day as derived from the visual fit quality. The color-coded date of the asterisks and SEDs in the insets demonstrates that the SEDs and clouds are locked in phase relative to each other for each storm even though the drift rates are slightly different from one storm to the next. This gives a strong evidence that the SEDs are produced by lightning in these clouds.

The phase shift between SED occurrence and cloud CM crossings is somewhat puzzling (Porco et al., 2005). Each Saturn's day the cloud rotates into the spacecraft-facing side of Saturn at a phase of 0.25 and rotates behind the horizon at a phase of 0.75 (see insets of Figs. 7 and 8). The SEDs would be expected to occur while the storm is on the spacecraft-facing side, i.e., from phase 0.25 to 0.75. Most of the 2004 SEDs start at around phase 0.1 and end at around 0.5–0.6. Most of the 2006 SEDs start at around phase 0.1 and end at around 0.75. Thus, both 2004 and 2006 SEDs start too early: around 0.15 of the rotation period earlier than the cloud becomes observable on the near side of the planet. Also, the 2004 SEDs end too early. As can be seen in the 2004 image of Saturn in Fig. 1, the cloud appears from behind the horizon (left side of Saturn) on the night side, then crosses the terminator and disappears behind the horizon on the day side (right side of Saturn). The 2006 observational geometry is similar except the illuminated crescent is smaller at the beginning of the storm and then slowly changes to about half-phase crescent at the end of the storm.

The early appearance of SEDs may be explained to some extent by an ionospheric propagation effect. The refraction of the SEDs by the night-side ionosphere has been modeled by Zarka et al. (2006), and can explain SED starting of the order of 0.1 to 0.2 rotation earlier than the cloud appears. Also, this model gives a qualitative explanation of the variation of the SED lower frequency cutoff, as discussed in companion paper by Fischer et al. (2007). The early turn off of the 2004 SEDs may be due to the day side ionospheric absorption (Fischer et al., 2006, 2007).

The SED/CM crossing phase shift is not completely understood by modeling, but the precise correlation of SEDs and clouds in timing and amplitudes on the timescale of days and years leaves small doubt about the lightning origin of the 2004 and 2006 SEDs.

6. Discussion

The night side images in Fig. 5 are part of the search for the direct detection of lightning flashes on Saturn. No flashes have been seen so far. This is not surprising because the clouds

and hazes above lightning on Saturn are expected to be very thick. Compared to Jupiter, water clouds expected to produce lightning should form much deeper [at 20 bars compared to 7 bars on Jupiter (Weidenschilling and Lewis, 1973)], which means an even larger column of atmosphere on Saturn because of its lower gravity. Additionally, the ring shine is bright at this time of the saturnian year and only extraordinarily bright lightning may compete with the brightness of the ring-illuminated clouds. Also, even if the lightning and ring-shine brightness were comparable, lightning-illuminated clouds are hard to distinguish from small highly reflective clouds. Even though we are convinced that the lightning occurred in the Fig. 5 clouds because we know of the correlation with radio signals, we cannot identify the flashes in the images.

We are looking forward to the observations of polar regions, where the rings are below the horizon, for possible flash detections. The Cassini extended mission may help in direct detection of lightning because at Saturn equinox on August 11, 2009 the Sun will cross the ring plane and the ringshine will be minimal.

The Cassini extended mission also is likely to bring important information about temporal changes in Saturn lightning (as visible reflective clouds, radio signals, or directly observed flashes), as we now know that lightning changes dramatically on the timescale of years. The extended mission is essential to see if those long timescales are connected to Saturn's seasons.

Acknowledgments

This research was supported by the NASA Cassini Project. The research at the University of Iowa was supported by NASA through Contract 1279973 with the Jet Propulsion Laboratory. U.D. thanks Ashwin Vasavada for the comments on the manuscript. We thank Don Banfield and another anonymous reviewer for their suggestions.

References

Burns, J.A., Showalter, M.R., Cuzzi, J.N., Durisen, R.H., 1983. Saturn's electrostatic discharges: Could lightning be the cause? Icarus 54, 280–295.

Del Genio, A.D., Kovari, W., 2002. Climatic properties of tropical precipitating convection under varying environmental conditions. J. Climate 15, 2597–2615.

Del Genio, A.D., Barbara, J.M., Ferrier, J., Ingersoll, A.P., West, R.A., Vasavada, A.R., Spitale, J., Porco, C.C., 2006. Saturn eddy momentum fluxes and convection: First estimates from Cassini images. Icarus, in press.

Dyudina, U.A., del Genio, A.D., Ingersoll, A.P., Porco, C.C., West, R.A., Vasavada, A.R., Barbara, J.M., 2004. Lightning on Jupiter observed in the H_α line by the Cassini imaging science subsystem. Icarus 172, 24–36.

Fischer, G., Desch, M.D., Zarka, P., Kaiser, M.L., Gurnett, D.A., Kurth, W.S., Macher, W., Rucker, H.O., Lecacheux, A., Farrell, W.M., Cecconi, B., 2006. Saturn lightning recorded by Cassini/RPWS in 2004. Icarus 183, 135–152.

Fischer, G., Kurth, W.S., Dyudina, U.A., Kaiser, M.L., Zarka, P., Lecacheux, A., Ingersoll, A.P., Gurnett, D.A., 2007. Analysis of a giant lightning storm on Saturn. Icarus, in press.

Gurnett, D.A., Kurth, W.S., Hospodarsky, G.B., Persoon, A.M., Averkamp, T.F., Cecconi, B., Lecacheux, A., Zarka, P., Canu, P., Cornilleau-Wehrlin, N., Galopeau, P., Roux, A., Harvey, C., Louarn, P., Bostrom, R., Gustafsson, G., Wahlund, J.-E., Desch, M.D., Farrell, W.M., Kaiser, M.L., Goetz, K., Kellogg, P.J., Fischer, G., Ladreiter, H.-P., Rucker, H., Alleyne, H., Pedersen, A., 2005. Radio and plasma wave observations at Saturn from Cassini's approach and first orbit. Science 307, 1255–1259.

Hueso, R., Sánchez-Lavega, A., 2004. A three-dimensional model of moist convection for the giant planets. II. Saturn's water and ammonia moist convective storms. Icarus 172, 255–271.

Kaiser, M.L., Connerney, J.E.P., Desch, M.D., 1983. Atmospheric storm explanation of saturnian electrostatic discharges. Nature 303, 50–53.

Kaiser, M.L., Desch, M.D., Kurth, W.S., Lecacheux, A., Genova, F., Pedersen, B.M., Evans, D.R., 1984. Saturn as a radio source. In: Gehrels, T., Matthews, M.S. (Eds.), Saturn. Univ. of Arizona Press, pp. 378–415.

Little, B., Anger, C.D., Ingersoll, A., Vasavada, A.R., Senske, D.A., Breneman, H.H., Borucki, W.J., the Galileo SSI Team, 1999. Galileo images of lightning on Jupiter. Icarus 142, 306–323.

MacGorman, D.R., Rust, W.D., 1998. The electrical nature of storms. Oxford Univ. Press, New York, Oxford.

Porco, C.C., West, R.A., Squyres, S., McEwen, A., Thomas, P., Murray, C.D., Delgenio, A., Ingersoll, A.P., Johnson, T.V., Neukum, G., Veverka, J., Dones, L., Brahic, A., Burns, J.A., Haemmerle, V., Knowles, B., Dawson, D., Roatsch, T., Beurle, K., Owen, W., 2004. Cassini Imaging Science: Instrument characteristics and anticipated scientific investigations at Saturn. Space Sci. Rev. 115, 363–497.

Porco, C.C., Baker, E., Barbara, J., Beurle, K., Brahic, A., Burns, J.A., Charnoz, S., Cooper, N., Dawson, D.D., Del Genio, A.D., Denk, T., Dones, L., Dyudina, U., Evans, M.W., Giese, B., Grazier, K., Helfenstein, P., Ingersoll, A.P., Jacobson, R.A., Johnson, T.V., McEwen, A., Murray, C.D., Neukum, G., Owen, W.M., Perry, J., Roatsch, T., Spitale, J., Squyres, S., Thomas, P., Tiscareno, M., Turtle, E., Vasavada, A.R., Veverka, J., Wagner, R., West, R., 2005. Cassini Imaging Science: Initial results on Saturn's atmosphere. Science 307, 1243–1247.

Sanchez-Lavega, A., Colas, F., Lecacheux, J., Laques, P., Parker, D., Miyazaki, I., 1991. The Great White Spot and disturbances in Saturn's equatorial atmosphere during 1990. Nature 353, 397–401.

Smith, B.A., Soderblom, L., Batson, R., Bridges, P., Inge, J., Masursky, H., Shoemaker, E., Beebe, R., Boyce, J., Briggs, G., Bunker, A., Collins, S.A., Hansen, C.J., Johnson, T.V., Mitchell, J.L., Terrile, R.J., Cook, A.F., Cuzzi, J., Pollack, J.B., Danielson, G.E., Ingersoll, A., Davies, M.E., Hunt, G.E., Morrison, D., Owen, T., Sagan, C., Veverka, J., Strom, R., Suomi, V.E., 1982. A new look at the Saturn system: The Voyager 2 images. Science 215, 505–537.

Sromovsky, L.A., Revercomb, H.E., Krauss, R.J., Suomi, V.E., 1983. Voyager 2 observations of Saturn's northern mid-latitude cloud features—Morphology, motions, and evolution. J. Geophys. Res. 88, 8650–8666.

Tomasko, M.G., West, R.A., Orton, G.S., Teifel, V.G., 1984. Clouds and aerosols in Saturn's atmosphere. In: Saturn. Univ. of Arizona Press, Tucson, AZ, pp. 150–194.

Vasavada, A.R., Hörst, S.M., Kennedy, M.R., Ingersoll, A.P., Porco, C.C., Del Genio, A.D., West, R.A., 2006. Cassini imaging of Saturn: Southern hemisphere winds and vortices. J. Geophys. Res. 111. E05004.

Weidenschilling, S.J., Lewis, J.S., 1973. Atmospheric and cloud structures of the jovian planets. Icarus 20, 465–476.

Westphal, J.A., Baum, W.A., Ingersoll, A.P., Barnet, C.D., de Jong, E.M., Danielson, G.E., Caldwell, J., 1992. Hubble Space Telescope observations of the 1990 equatorial disturbance on Saturn—Images, albedos, and limb darkening. Icarus 100, 485–498.

Zarka, P., Cecconi, B., Denis, L., Farrell, W.M., Fischer, G., Hospodarsky, G.B., Kaiser, M.L., Kurth, W.S., 2006. Physical properties and detection of Saturn's radio lightning. In: Rucker, H.O., Kurth, W.S., Mann, G. (Eds.), Planetary Radio Emissions VI. Austrian Academy of Sciences Press, Vienna, pp. 111–122.